Complexity Results and Fast Methods for Optimal Tabletop Rearrangement with Overhand Grasps

Shuai D Han, Nicholas M Stiffler, Athanasios Krontiris, Kostas E Bekris, and Jingjin Yu

arXiv:1711.07369v1 [cs.RO] 17 Nov 2017

Abstract—This paper studies the underlying combinatorial structure of a class of object rearrangement problems, which appear frequently in applications. The problems involve multiple, similar-geometry objects placed on a flat, horizontal surface, where a robot can approach them from above and perform pick-and-place operations to rearrange them. The paper considers both the case where the start and goal object poses overlap, and where they do not. For overlapping poses, the primary objective is to minimize the number of pick-and-place actions and then to minimize the distance traveled by the end-effector. For the non-overlapping case, the objective is solely to minimize the travel distance of the end-effector. While such problems do not involve all the complexities of general rearrangement, they remain computationally hard in both cases. This is shown through reductions from well-understood, hard combinatorial challenges to these rearrangement problems. The reductions are also shown to hold in the reverse direction, which enables the convenient application on rearrangement of well studied algorithms. These algorithms can be very efficient in practice despite the hardness results. The paper builds on these reduction results to propose an algorithmic pipeline for dealing with the rearrangement problems. Experimental evaluation, including hardware-based trials, shows that the proposed pipeline computes high-quality paths with regards to the optimization objectives. Furthermore, it exhibits highly desirable scalability as the number of objects increases in both the overlapping and non-overlapping setup.

I. INTRODUCTION

In many industrial and logistics applications, such as those shown in Fig. 1, a robot is tasked to rearrange multiple, similar objects placed on a tabletop into a desired arrangement. In these setups, the robot needs to approach the objects from above and perform a *pick-and-place action* at desired target poses. Such operations are frequently part of product packaging and inspection processes. Efficiency plays a critical role in these domains, as the speed of task completion has a direct impact on financial viability; even a marginal improvement in productivity could provide significant competitive advantage in practice. Beyond industrial robotics, a home assistant robot may need to deal with such problems as part of a room cleaning task. The reception of such a robot by people will be more positive if its solutions are efficient and the robot does not waste time performing redundant actions. Many subtasks affect the efficiency of the overall solution in all of these applications, ranging from perception to the robot's speed in grasping and transferring objects. But overall efficiency also critically depends on the underlying combinatorial aspects of the problem, which relate to the number of pick-and-place actions that the robot performs, the placement of the objects, as well as the sequence of objects transferred.

This paper deals with the combinatorial aspects of tabletop

Fig. 1. Examples of robots deployed in industrial settings tasked to arrange objects in desired configurations through pick and place: (left) ABB's IRB 360 FlexPicker rearranging pancakes (right) Stäubli's TP80 Fast Picker robot.

object rearrangement tasks. The objective is to understand the underlying structure and obtain high-quality solutions in a computationally efficient manner. The focus is on a subset of general rearrangement problems, which relate to the above mentioned applications. In particular, the setup corresponds to rearranging multiple, similar-geometry, non-stacked objects on a flat, horizontal surface from given initial to target arrangements. The robot can approach the objects from above, pick them up and raise them. At that point, it can move them freely without collisions with other objects.

There are two important variations of this problem. The first requires that the target object poses do not overlap with the initial ones. In this scenario, the number of pick-and-place actions is equal to the number of objects not in their goal pose. Thus, the solution quality is dependent upon the sequence with which the objects are transferred. A good sequence can minimize the distance that the robot's end-effector travels. The second variant of the problem allows for target poses to overlap with the initial poses, as in Fig. 2a-c. The situation sometimes necessitates the identification of intermediate poses for some objects to complete the task. In such cases, the quality of the solution tends to be dominated by the number of intermediate poses needed to solve the problem, which correlates to the number of pick-and-place actions the robot must carry out. The primary objective is to find a solution, which uses the minimum number of intermediate poses and among them minimize the distance the robot's end-effector travels.

Both variations include some assumptions that simplify these instances relative to the general rearrangement problem. The non-overlapping case in particular seems to be quite easy since a random feasible solution can be trivially acquired. Nevertheless, this paper shows that even in this simpler setup, the optimal variant of the problem remains computationally hard. This is achieved by reducing the Euclidean-`TSP` problem [1] to the cost-optimal, non-overlapping tabletop object rearrangement problem. Even in the unlabeled case, where

objects can occupy any target pose, the problem is still hard. For overlapping initial and final poses, the paper employs a graphical representation from the literature [2], which leads to the result that finding the minimum number of pick-and-place actions relates to a well-known problem in the algorithmic community, the "Feedback Vertex Set" (FVS) problem [3]. This again indicates the hardness of the challenge.

The benefit of these two-way reductions, beyond the hardness results themselves, is that they suggest algorithmic solutions and provide an expectation on the practical efficiency of the methods. In particular, Euclidean-TSP admits a polynomial-time approximation scheme (PTAS) and good heuristics, which implies very good practical solutions for the non-overlapping case. On the other hand, the FVS problem is APX-hard [3], [5], which indicates that efficient algorithms are harder for the overlapping case. This motivated the consideration of alternative heuristics for solving such challenges that make sense in the context of object rearrangement.

The algorithms proposed here, which arose by mapping the object rearrangement variations to well-studied problems have been evaluated in terms of practical performance. For the non-overlapping case, an alternative solver exists that was developed for a related challenge [6]. The TSP solvers achieve superior performance relative to this alternative when applied to object rearrangement. They achieve sub-second solution times for hundreds of objects. Optimal solutions are shown to be significantly better than the average, random, feasible solution. For the overlapping case, exact and heuristic solvers are considered. The paper shows that practically efficient methods achieve sub-second solution times without a major impact in solution quality for tens of objects.

This article expands an earlier version of this work [7] and includes the following new contributions: *(i)* a proof showing that cost-optimal unlabelled non-overlapping tabletop rearrangement is NP-hard, *(ii)* a complete description of ILP-based heuristics and an algorithm for solving the object rearrangement problem with overlap sub-optimally, *(iii)* significantly enhanced evaluation with experiments conducted on a hardware platform (Fig. 2d), corroborating the real-world benefits of the proposed method.

The structure of this manuscript is as follows. Section II reviews related work, followed by a formal problem statement in Section III. Section IV considers the object rearrangement problem when the objects have non-overlapping start and goal arrangements. The more computationally challenging problem that involves overlapping start and goal arrangements appears in Section V. The evaluation of the proposed methods is broken down into two components: simulation (Section VI) and physical experiments (Section VII). The paper concludes with a summary and remarks about future directions in Section VIII.

II. CONTRIBUTION RELATIVE TO PRIOR WORK

Multi-body planning is a related challenge that is itself hard. In the general, continuous case, complete approaches do not scale even though methods exist that try to decrease the effective DOFs [8]. For specific geometric setups, such as unlabeled unit-discs among polygonal obstacles, optimality

can be achieved [9], even though the unlabeled case is still hard [10]. Given the hardness of multi-robot planning, decoupled methods, such as priority-based schemes [11] or velocity tuning [12], trade completeness for efficiency. Assembly planning [13], [14], [15] deals with similar problems but few optimality arguments have been made.

Recent progress has been achieved for the discrete variant of the problem, where robots occupy vertices and move along edges of a graph. For this problem, also known as "pebble motion on a graph" [16], [17], [18], [19], feasibility can be answered in linear time and paths can be acquired in polynomial time. The optimal variation is still hard but recent optimal solvers with good practical efficiency have been developed either by extending heuristic search to the multi-robot case [20], [21], or utilizing solvers for other hard problems, such as network-flow [22], [23]. The current work is motivated by this progress and aims to show that for certain useful rearrangement setups it is possible to come up with practically efficient algorithms through an understanding of the problem's structure.

Navigation among Movable Obstacles (NAMO) is a related computationally hard problem [24], [25], [26], [27], where a robot moves and pushes objects. A probabilistically complete solution exists for this problem [28]. NAMO can be extended to manipulation among movable obstacles (MAMO) [29] and rearrangement planning [30], [31]. Monotone instances for such problems, where each obstacle may be moved at most once, are easier [29]. Recent work has focused on "non-monotone" instances [32], [33], [34], [35], [36], [37]. Rearrangement with overlaps considered in the current paper includes "non-monotone" instances although other aspects of the problem are relaxed. In all these efforts, the focus is on feasibility and no solution quality arguments have been provided. Asymptotic optimality has been achieved for the related "minimum constraint removal" path problem [38], which, however, does not consider negative object interactions.

The *Pickup and Delivery Problem* (PDP) [39], [40] is a well-studied problem in operations research that is similar to tabletop object rearrangement, as long as the object geometries are ignored. The PDP models the pickup and delivery of goods between different parties and can be viewed as a subclass of vehicle routing [41] or dispatching [42]. It is frequently specified over a graph embedded in the 2D plane, where a subset of the vertices are pickup and delivery locations. A PDP in which pickup and delivery sites are not uniquely paired is also known as the NP-hard swap problem [43], [44], for which a 2.5-optimal heuristic is known [44]. Many exact linear programming algorithms and approximations are available [45], [46], [47] when pickup and delivery locations overlap, where pickup must happen some time after delivery. The stacker crane problem (SCP) [48], [6] is a variation of PDP of particular relevance as it maps to the non-overlapping case of labeled object rearrangement. An asymptotically optimal solution for SCP [6] is used as a comparison point in the evaluation section.

This work does not deal with other aspects of rearrangement, such as arm motion [49], [50], [51], [52] or grasp planning [53], [54]. Non-prehensile actions, such as pushing,
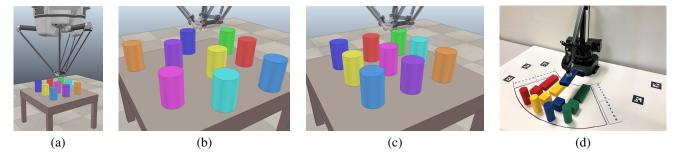
Fig. 2. (a, b, c) An example of an object rearrangement challenge considered in this work from a V-REP simulation [4], where the initial (b) and final (c) object poses are overlapping and an object needs to be placed at an intermediate location. (d) In addition to the V-REP simulations, the solutions presented in this work have been tested on an experimental hardware platform.

are also not considered [55], [56]. Similar combinatorial issues to the ones studied here are also studied by integrated task and motion planners, for most of which there are no optimality guarantees [57], [58], [33], [34], [59], [60]. Recent work on asymptotically optimal task planning is at this point prohibitively expensive for practical use [61].

III. PROBLEM STATEMENT

This section formally defines the considered challenges.

A. Tabletop Object Rearrangement with Overhand Grasps

Consider a workspace $\mathcal{W}$ with static obstacles and a set of n movable objects $\mathcal{O} = \{o_1, \ldots, o_n\}$. For $o_i \in \mathcal{O}$, $\mathcal{C}_i$ denotes its configuration space. Then, $\mathcal{F}_i \subseteq \mathcal{C}_i$ is the set of collision-free configurations of o_i with respect to the static obstacles in $\mathcal{W}$. An *arrangement* $R = \{r_1, \ldots, r_n\}$ for the objects $\mathcal{O}$ specifies the configurations $r_i \in \mathcal{C}_i$ for each object o_i. A feasible arrangement is one satisfying:

1) $\forall\ r_i \in R, r_i \in \mathcal{F}_i$;
2) $\forall\ r_i, r_j \in R$, if $i \neq j$, then objects o_i and o_j are not in collision when placed at r_i and r_j, respectively.

This work focuses on closed and bounded planar workspaces: $\mathcal{W} \subset \mathbb{R}^2$. The setting is frequently referred to as the *tabletop* setup, in which the vertical projections of the objects on the tabletop do not intersect. This work assumes that the manipulator is able to employ *overhand* grasps, where an object can be transferred after being lifted above all other objects. In particular, a pick-and-place operation of the manipulator involves four steps:

a. bringing the end-effector above the object,
b. grasping and lifting the object,
c. transfer of the grasped object horizontally to its target (horizontal) location, and
d. a downward motion prior to releasing the object.

This sequence constitutes a *manipulation action*.

The manipulator is initially at a rest position s_M prior to executing any pick-and-place actions and transitions to a rest position g_M at the conclusion of the rearrangement task. A *rest position* is a safe arm configuration, where there is no collision with objects.

The illustrations that appear throughout the paper assume objects with identical geometry. Nevertheless, the results de-

rived in this paper are not dependent on this assumption, i.e., objects need only be general cylinders.[1]

Given the setup, the problem studied in the paper can be summarized as:

Problem 1. *Tabletop Object Rearrangement with Overhand grasps (*TORO*). Given feasible start and goal arrangements R_S, R_G for objects $\mathcal{O} = \{o_1, \ldots, o_n\}$ on a tabletop, determine a sequence of collision-free pick-and-place actions with overhand grasps $\mathcal{A} = (a^1, a^2, \ldots)$ that transfer $\mathcal{O}$ from R_S to R_G.*

A rearrangement problem is said to be *labeled* if objects are unique and not interchangeable. Otherwise, the problem is *unlabeled*. If for two arbitrary arrangements $s \in R_S$ and $g \in R_G$, the objects placed in s and g are not in collision, then the problem is said to have *no overlaps*. Otherwise, the problem is said to have *overlaps*.

This paper primarily focuses on the labeled TORO case and identifies an important subcase:

- TORO *with NO overlaps (*TORO-NO*)*

Remark 1. The partition of Problem 1 into the general TORO case and the subcase of TORO-NO is not arbitrary. TORO is structurally richer and harder from a computational perspective. Both versions of the problem can be extended to the unlabeled and partially labeled variants. This paper does not treat the labeled and unlabeled variants as separate cases but will briefly discuss differences that arise due to formulation when appropriate.

B. Optimization Criteria

Recall that a manipulation action a^i has four components: an initial move, a grasp, a transport phase, and a release. Since grasping is frequently the source of difficulty in object manipulation tasks, it is assumed in the paper that grasps and subsequent releases induce the most cost in manipulation actions. The other source of cost can be attributed to the length of the manipulator's path. This part of the cost is captured through the Euclidean distance traveled by the end effector between grasps and releases. For a manipulation action a^i, the incurred cost is

$$c_{a^i} = c_m d_e^i + c_g + c_m d_l^i + c_r, \tag{1}$$

---

[1]From differential geometry, a cylinder is defined as any ruled surface spanned by a one-parameter family of parallel lines.

where c_m, c_g, c_r are costs associated with moving the manipulator, a single grasp, and a single release, respectively. d_e^i and d_l^i are the straight line distances traveled by the end effector in the first (object-free) and third (carrying an object) stages of a manipulation action, respectively.

The total cost associated with solving a TORO instance is then captured by

$$c_T = \sum_{i=1}^{|\mathcal{A}|} c_{a^i} = |\mathcal{A}|(c_g + c_r) + c_m\Big(\sum_{i=1}^{|\mathcal{A}|}(d_e^i + d_l^i) + d_f\Big), \quad (2)$$

where d_f is the distance between the location of the last release of the end effector and its rest position g_M. Of the two additive terms in (2), note that the first term dominates the second. Because the absolute value of c_g, c_r, and c_m are different for different systems, the assignment of their absolute values is left to practitioners. The focus of this paper is the analysis and minimization of the two additive terms in (2).

C. Object Buffer Locations

The resolution of TORO (Section V) may require the temporary placement of some object(s) at intermediate locations outside those in $R_S \cup R_G$. When this occurs, external buffer locations may be used as temporary locations for object placement. More formally, there exists a set of configurations $B = \{b_1, b_2, \dots\}$, called *buffers*, which are available to the manipulator and do not overlap with object placements in R_S or R_G.

Remark 2. This work, which focuses on the combinatorial aspects of multi-object manipulation and rearrangement, utilizes exclusively buffers that are not on the tabletop. It is understood that the number of external buffers *may* be reduced by attempting to first search for potential buffers within the tabletop. Nevertheless, there are scenarios where the use of external buffers may be necessary.

IV. TORO WITH NO OVERLAPS (TORO-NO)

When there is no overlap between any pair of start and goal configurations, an object can be transferred directly from its start configuration to its goal configuration. A direct implication is that an optimal sequence of manipulation actions contains exactly $|\mathcal{A}| = |\mathcal{O}| = n$ grasps and the same number of releases. Note that a minimum of n grasps and releases are necessary. This also implies that no buffer is required since using buffers will incur additional grasp and release costs. Therefore, for TORO-NO, (2) becomes

$$c_T = n(c_g + c_r) + c_m\Big(\sum_{i=1}^{n}(d_e^i + d_l^i) + d_f\Big), \quad (3)$$

i.e., only the distance traveled by the end effector affects the cost. The problem instance that minimizes (3) is referred to as Cost-optimal TORO-NO. The following theorem provides a hardness result for Cost-optimal TORO-NO.

Theorem IV.1. *Cost-optimal* TORO-NO *is NP-hard.*

Proof: Reduction from Euclidean-TSP [1]. Let $p_0, p_1, \dots, p_n$ be an arbitrary set of $n+1$ points in 2D. The set of points induces an Euclidean-TSP. Let d_{ij} denote the

Euclidean distance between p_i and p_j for $0 \leq i, j \leq n$. In the formulation given in [1], it is assumed that d_{ij} are integers, which is equivalent to assuming the distances are rational numbers. To reduce the stated TSP problem to a cost-optimal TORO-NO problem, pick some positive $\varepsilon \ll 1/(4n)$. Let p_0 be the rest position of the manipulator in an object rearrangement problem. For each p_i, $1 \leq i \leq n$, split p_i into a pair of start and goal configurations (s_i, g_i) such that *(i)* $p_i = \frac{s_i + g_i}{2}$, *(ii)* $s_{i2} = g_{i2}$, and *(iii)* $s_{i1} + \varepsilon = g_{i1}$. An illustration of the reduction is provided in Fig. 3. The reduced TORO-NO instance is fully defined by p_0, $R_S = \{s_1, \dots, s_n\}$ and $R_G = \{g_1, \dots, g_n\}$. A cost-optimal (as defined by (3)) solution to this TORO-NO problem induces a (closed) path starting from p_0, going through each s_i and g_i exactly once, and ending at p_0. Moreover, each g_i is visited immediately after the corresponding s_i is visited. Based on this path, the manipulator moves to a start location to pick up an object, drop the object at the corresponding goal configuration, and then move to the next object until all objects are rearranged. Denote the loop path as P and let its total length be D.
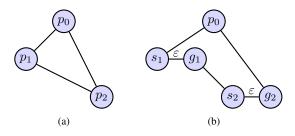

Fig. 3. Reduction from Euclidean-TSP to cost-optimal TORO-NO

Assume that the Euclidean-TSP has an optimal solution path P_{opt} with a total distance of D_{opt} (an integer). Then P from solving the cost-optimal TORO-NO yields such an optimal path for the TSP. To show this, from P, simply contract the edges $s_i g_i$ for all $1 \leq i \leq n$. This clearly yields a solution to the Euclidean-TSP; let the resulting path be P' with total length D'. As edges are contracted along P, by the triangle inequality, $D' \leq D$. It remains to show that $D' = D_{opt}$. Suppose this is not the case, then $D' \geq D_{opt} + 1$. However, if this is the case, a solution to the TORO-NO can be constructed by splitting p_i into s_i and g_i along P_{opt}. It is straightforward to establish that the total distance of this TORO-NO path is bounded by $D_{opt} + n\varepsilon < D_{opt} + n * 1/(4n) = D_{opt} + 1/4 < D_{opt} + 1 \leq D' \leq D$. Since this is a contradiction, $D' = D_{opt}$. ∎

Remark 3. Note that an NP-hardness proof of a similar problem can be found in [62], as is mentioned in [6]. Nevertheless, the problem is stated for a tree and is non-Euclidean. Furthermore, it is straightforward to show that the decision version of the cost-optimal TORO-NO problem is NP-complete; the detail, which is non-essential to the focus of the current paper, is omitted.

Remark 4. Interestingly, TORO-NO may also be reduced to a variant of TSP with very little overhead. Because highly efficient TSP solvers are available, the reduction route provides an effective approach for solving TORO-NO. That is, an TORO-NO instance may be reduced to TSP and solved, with the TSP solution readily translated back to a solution

to the `TORO-NO` instance that is cost-optimal. This is not always a feature of NP-hardness reductions. The straightforward algorithm for the computation is outlined in Alg. 1. The inputs to the algorithm are the rest positions of the manipulator and the start and goal configurations of objects. The output is the solution for `TORO-NO`, represented as a sequence of manipulation actions $\mathcal{A}$, which has completeness and optimality guarantees.

Algorithm 1: TORONOTSP

Input: Configurations s_M, g_M, Arrangements R_S, R_G.
Output: A sequence of manipulation actions $\mathcal{A}$.
1 $G_{NO} \leftarrow$ CONSTRUCTTSPGRAPH(R_S, R_G, s_M, s_G)
2 $S_{raw} \leftarrow$ SOLVETSP(G_{NO})
3 $\mathcal{A} \leftarrow$ RETRIEVEACTIONS(S_{raw})
4 **return** $\mathcal{A}$

At Line 1 of Alg. 1, a graph $G_{NO}(V_{NO}, E_{NO})$ is generated as the input to the `TSP` problem. The graph is constructed from the `TORO-NO` instance as follows. A vertex is created for each element of R_S and R_G. Then, a complete bipartite graph is created between these two sets of vertices. A set of vertices $U = \{u_1, \ldots, u_{|R_S|}\}$ is then inserted into edges $s_i g_i$ for $1 \leq i \leq |R_S|$. Afterward, s_M (resp., g_M) is added as a vertex and is connected to s_i (resp., g_i) for $1 \leq i \leq |R_S|$. Finally, a vertex u_0 is added and connected to both s_M and g_M. See Fig. 4 for the straightforward example for $|R_S| = 2$.
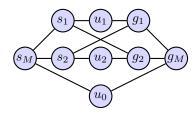

Fig. 4. An example of G_{NO} for 2 objects. The nodes s_M and g_M denote the initial and final rest positions of the manipulator end effector.

Let $w(a, b)$ denote the weight of an edge $(a, b) \in E_{NO}$. For all $1 \leq i, j \leq n, i \neq j$ (dist(x, y) denotes the Euclidean distance between x and y in 2D):

$$w(s_M, u_0) = w(g_M, u_0) = 0, w(s_M, s_i) = \text{dist}(s_M, s_i),$$
$$w(g_M, g_i) = \text{dist}(g_M, g_i), w(s_i, u_i) = w(u_i, g_i) = 0,$$
$$w(s_i, g_j) = \text{dist}(s_i, g_j).$$

With the construction, a `TSP` tour through G_{NO} must use $s_M u_0 g_M$ and all $s_i u_i g_i$ for all $1 \leq i \leq |R_S|$. To form a complete tour, exactly $(|R_S| - 1)$ edges of the form $g_i s_j$, where $i \neq j$ must be used. At Line 2, the `TSP` is solved (using Concorde `TSP` solver [63]). This yields a minimum weight solution S_{raw}, which is a cycle containing all $v \in V_{NO}$. The manipulation actions can then be retrieved (Line 3).

An alternative solution to `TORO-NO` could employ the asymptotically optimal, *SPLICE* algorithm, introduced in [6].

A. Unlabelled `TORO-NO`

The scenario where objects are unlabeled is a special case of `TORO-NO` which has significance in real-world applications (e.g., the pancake stacking application). This case is denoted as `TORO-UNO` (unlabeled, no overlap). Adapting the NP-hardness proof for the `TORO-NO` problem shows that cost-optimal `TORO-UNO` is also NP-hard. Similar to the `TORO-NO` case, the optimal solution only hinges on the distance traveled by the manipulator because no buffer is required and exactly n grasps and releases are needed.

Theorem IV.2. *Cost-optimal* `TORO-UNO` *is NP-hard.*
Proof: See Appendix A. ∎

When solving a `TORO-UNO` instance, Alg. 1 may be used with a few small changes. First, a different underlying graph must be constructed. Denote the new graph as $G_{UNO}(V_{UNO}, E_{UNO})$, where $V_{UNO} = R_S \cup R_G \cup \{s_M, u_0, g_M\}$. For all $1 \leq i, j \leq n$:

$$w(s_M, u_0) = w(g_M, u_0) = 0, w(s_M, s_i) = \text{dist}(s_M, s_i),$$
$$w(g_M, g_i) = \text{dist}(g_M, g_i), w(s_i, g_j) = \text{dist}(s_i, g_j).$$

All other edges are given infinite weight. An example of the updated structure of G_{UNO} for two objects is illustrated in Fig. 5.
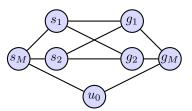

Fig. 5. An example of G_{UNO} for 2 objects.

V. TORO WITH OVERLAP (TORO)

Unlike `TORO-NO`, `TORO` has a more sophisticated structure and may require buffers to solve. In this section, a *dependency graph* [2] is used to model the structure of `TORO`, which leads to a classical NP-hard problem known as the *feedback vertex set* problem [3]. The connection then leads to a complete algorithm for optimally solving `TORO`.

A. The Dependency Graph and NP-Hardness of `TORO`

Consider a *dependency digraph* $G_{dep}(V_{dep}, A_{dep})$, where $V_{dep} = \mathcal{O}$, and $(o_i, o_j) \in A_{dep}$ iff g_i and s_j overlap. Therefore, o_j must be moved away from s_j before moving o_i to g_i. An example involving two objects is provided in Fig. 6. The definition of dependency graph implies the following two observations.

Observation V.1. *If the out-degree of $o_i \in V_{dep}$ is 0, then o_i can move to g_i without collision.*

Observation V.2. *If G_{dep} is not acyclic, solving* `TORO` *requires at least $n + 1$ grasps.*

The dependency graph has obvious similarities to the well known *feedback vertex set* (`FVS`) problem [3]. A directed `FVS` problem is defined as follows. Given a strongly connected
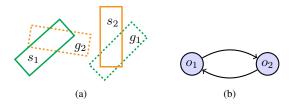
Fig. 6. Illustration of the dependency graph. (a) Two objects are to be moved from s_i to g_i, $i = 1, 2$. Due to the overlap between s_1 and g_2 as well as the overlap between s_2 and g_1, one of the objects must be temporarily moved aside. (b) The dependency graph capturing the scenario in (a).

directed graph $G = (V, A)$, an FVS is a set of vertices whose removal leaves G acyclic. Minimizing the cardinality of this set is NP-hard, even when the maximum in degree or out degree is no more than two [43]. As it turns out, the set of removed vertices in an FVS problem mirrors the set of objects that must be moved to temporary locations (i.e., buffers) for resolving the dependencies between the objects, which corresponds to the additional grasps (and releases) that must be performed in addition to the n required grasps for rearranging n objects. The observation establishes that cost-optimal TORO is also computationally intractable. The following lemma shows this point.

Lemma V.1. *Let the dependency graph of a* TORO *problem be a single strongly connected graph. Then the minimum number of additional grasps required for solving the* TORO *problem equals the cardinality of the minimum FVS of the dependency graph.*

Proof: Given the dependency graph, let the additional grasps and releases be n_x and the minimum FVS have a cardinality of n_{fvs}, it remains to show that $n_x = n_{fvs}$. First, if fewer than n_{fvs} objects are removed, which correspond to vertices of the dependency graph, then there remains a directed cycle. By Observation V.2, this part of the problem cannot be solved. This establishes that $n_x \geq n_{fvs}$. On the other hand, once all objects corresponding to vertices in a minimum FVS are moved to buffer locations, the dependency graph becomes acyclic. This allows the remaining objects to be rearranged. This operation can be carried out iteratively with objects whose corresponding vertices have no incoming edges. On a directed acyclic graph (DAG), there is always such a vertex. Moreover, as such a vertex is removed from a DAG, the remaining graph must still be a DAG and therefore must have either no vertex (a trivial DAG) or a vertex without incoming edges. ∎

For dependency graphs with multiple strongly connected components, the required number of additional grasps and releases is simply the sum of the required number of such actions for the individual strongly connected components.

For a fixed TORO problem, let n_{fvs} be the cardinality of the largest (minimal) FVS computed over all strongly connected components of its dependency graph. Then it is easy to see that the maximum number of required buffers is no more than n_{fvs}. The NP-hardness of cost-optimal TORO is established using the reduction from FVS problems to TORO. This is more involved than reducing TORO to FVS because the constructed TORO must correspond to an actual TORO problem in which the number of overlaps should not grow unbounded.

Theorem V.1. *Cost-optimal* TORO *is NP-hard.*

Proof: The FVS problem on directed graphs is reduced to cost-optimal TORO. An FVS problem is fully defined by specifying an arbitrary strongly connected directed graph $G = (V, A)$ where each vertex has no more than two incoming and two outgoing edges. A typical vertex neighborhood can be represented as illustrated in Fig. 7(a). Such a neighborhood is converted to a dependency graph neighborhood of object rearrangement as follows. Each of the original vertex $v_i \in V$ becomes an object o_i which has some (s_i, g_i) pair as its start and goal configurations. For each directed arc $v_i v_j$, split it into two arcs and add an additional object o_{ij}. That is, create new arcs $o_i o_{ij}$ and $o_{ij} o_j$ for each original arc v_{ij} (see Fig. 7(b)). This yields a dependency graph that is again strongly connected. Two claims will be proven:

1) The constructed dependency graph corresponds to an object rearrangement problem, and
2) The minimum number of objects that must be moved away temporarily to solve the problem is the same as the size of the minimum FVS.
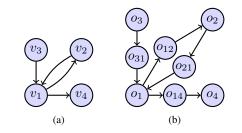

Fig. 7. Converting a neighborhood of a graph for an FVS problem to parts of a dependency graph for a TORO problem.

To prove the first claim, assume without loss of generality that the objects have the same footprints on the tabletop. Furthermore, only the neighborhood of o_1 needs to be inspected because it is isolated by the newly added objects. Recall that an incoming edge to o_1 means that the start configuration o_1 blocks the goals of some other objects, in this case o_{21} and o_{31}. This can be readily realized by putting the goal configurations of o_{21} and o_{31} close to each other and have them overlap with the start configuration of o_1. Note that the goal configurations of o_{21} and o_{31} have no other interactions. Therefore, such an arrangement is always achievable for even simple (e.g., circular or square) footprints. Similarly, for the outgoing edges from o_1, which mean other objects block o_1's goal, in this case o_{12} and o_{14}, place the start configurations of o_{12} and o_{14} close to each other and make both overlap with the goal configuration of o_1. Again, the start configurations of o_{12} and o_{14} have no other interactions.

The second claim directly follows Lemma V.1. Now, given an optimal solution to the reduced TORO problem, it remains to show that the solution can be converted to a solution to the original FVS problem. The solution to the TORO problem provides a set of objects that are moved to temporary locations. This yields a minimum FVS on the dependency graph but not the original graph G. Note that if a newly created object (e.g., o_{ij}) is moved to a temporary place, either object o_i or o_j can be moved since this will achieve no less in disconnecting the

dependency graph. Doing this across the dependency graph yields a minimum FVS for G. ∎

Remark 5. It is possible to prove that `TORO` is NP-hard using a similar proof to the `TORO-NO` case. To make the proof for Theorem IV.1 work here, each p_i can be split into an overlapping pair of start and goal. Such a proof, however, would bury the true complexity of `TORO`, which is a much more difficult problem. Unlike the Euclidean-`TSP` problem, which admits $(1+\varepsilon)$-approximations and good heuristics, `FVS` problems are `APX`-hard [3], [5].

B. Algorithmic Solutions for `TORO`

1) Feasible algorithm: Once the link between a `TORO` buffer requirement and `FVS` is established, an algorithm for solving `TORO` becomes possible. To do this, an FVS set is found. Then the optimal rearrangement distance is computed for this FVS set. The procedure for doing this is outlined in TOROFVSSINGLE (Alg. 2). At Line 1, the dependency graph G_{dep} is constructed. At Line 3-4, an FVS is obtained for each strongly connected component (SCC) in G_{dep}. Note that if these FVSs are optimal, then the step yields the minimum number of required grasps (and releases) as: $\min |\mathcal{A}| = n + |B|$.

The residual work is to find the solution with $n+|B|$ grasps and the shortest travel distance (Line 5). The manipulation actions are then retrieved and returned.

Algorithm 2: TOROFVSSINGLE

Input: Configurations s_M, g_M, Arrangements R_S, R_G
Output: A set of manipulation actions $\mathcal{A}$
1   $G_{dep} \leftarrow$ CONSTRUCTDEPGRAPH(R_S, R_G)
2   $B \leftarrow \emptyset$
3   **for** *each SCC in* G_{dep} **do**
4     $\lfloor \;\; B \leftarrow B \cup$ SOLVEFVS(SCC)
5   $S_{raw} \leftarrow$ MINDIST$(s_M, g_M, R_S, R_G, G_{dep}, B)$
6   $\mathcal{A} \leftarrow$ RETRIEVEACTIONS(S_{raw})
7   **return** $\mathcal{A}$

The paper explores two exact and three approximate methods as implementations of SOLVEFVS() (Line 4 of Alg. 2). The two exact methods are both based on integer linear programming (ILP) models, similar to those introduced in [64]. They differ in how cycle constraints are encoded: one uses a polynomial number of constraints and the other simply enumerates all possible cycles. Denote these two exact methods as **ILP-Constraint** and **ILP-Enumerate**, respectively. The details of these two exact methods are explained in Appendix A. With regards to approximate solutions, several heuristic solutions are presented:

1) **Maximum Simple Cycle Heuristic (MSCH)**. The FVS is obtained by iteratively removing the node that appears on the most number of simple cycles in G_{dep} until no more cycles exist. The simple cycles are enumerated.

2) **Maximum Cycle Heuristic (MCH)**. This heuristic is similar to MSCH but counts cycles differently. For each vertex $v \in V_{dep}$, it finds a cycle going through v and marks the outgoing edge from v on this cycle. The

process is repeated for v until no more cycles can be found. The vertex with the largest cycle count is then removed first.

3) **Maximum Degree Heuristics (MDH)**. This heuristic constructs an FVS through vertex deletion based on the degree of the vertex until no cycles exist.

Based on FVS, the solution minimizing travel distance can be found by MINDIST() (line 5), which is an LP modeling method inspired by [23] and described in Appendix A.

2) Complete algorithm: Note that TOROFVSSINGLE() is a complete algorithm for solving `TORO` but it is not a complete algorithm for solving `TORO` optimally. With some additional engineering, a complete optimal `TORO` solver can also be constructed: under the assumption that grasping dominates the traveling costs, simply iterate through all optimal FVS sets and then compute the subsequent minimum distance. After all such solutions are obtained, the optimal among these are chosen. It turns out that doing this enumeration does not provide much gain in solution quality as the optimal distances are very similar to each other.

VI. PERFORMANCE EVALUATION OF SIMULATIONS

All simulations are executed on an Intel(R) Core(TM) i7-6900K CPU with 32GB RAM at 2133MHz. Concorde [63] is used for solving the `TSP` and Gurobi 6.5.1 [65] for ILP models.

A. TORO-NO: Minimizing the Travel Distance

To evaluate the effectiveness of TORONOTSP, random `TORO-NO` instances are generated in which the number of objects varies. For each choice of number of objects, 100 instances are tried and the average is taken. Although TORONOTSP works on thousands of objects (it takes less than 30 seconds for TORONOTSP to solve instances with 2500 objects), the evaluation is limited to 200 objects[2]. Concerning running time, TORONOTSP is compared with *SPLICE* [6] which does not compute an exact optimal solution. As shown in Fig. 8, it takes less than a second for TORONOTSP to compute the distance optimal manipulation action set. Fig. 9
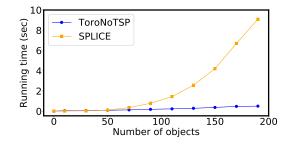

Fig. 8. Running time comparison of TORONOTSP and *SPLICE*.

illustrates the solution quality of TORONOTSP, *SPLICE*, and an algorithm that picks a random feasible solution. Notice that the random feasible solution generally has poor quality.

---

[2]State-of-the-art Delta robots have comparable abilities. For example, the Kawasaki YF03 Delta Robot is capable of performing 222 pick-and-place actions per minute (1kg objects).

TABLE I
EVALUATION OF THE TSP MODEL FOR THE UNLABELED CASE.

Number of objects	10	50	100	200
Running time (sec)	0.04	0.58	2.43	7.30
Optimality of random solution	1.94	3.72	4.92	6.01

SPLICE does well as the number of objects increases, but under-performs compared to TORONOTSP. In conclusion, TORONOTSP provides the best performance on both running time and optimality for practical sized TORO-NO problems.
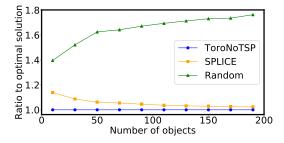

Fig. 9.   Optimality of TORONOTSP, *SPLICE* and a random selection method.

For the unlabeled case (TORO-UNO), the same experiments are carried out. The results appear in Table I. Note that *SPLICE* no longer applies. The last line of the table is the optimality of random solutions, included for reference purposes. For larger cases, the TSP based method is able to solve for over 500 objects in 30 seconds.

B. TORO: Minimizing the Number of Grasps

To evaluate different FVS minimization methods, dependency graphs are generated by capping the average degree and maximum degree for a fixed object count. To evaluate the running time, the average degree is set to 2 and the maximum degree is set to 4, which creates significant dependencies. The running time comparison is given in Fig. 10 (averaged over 100 runs per data point). Although exact ILP-based methods took more time than heuristics, they can solve optimally for over 30 objects in just a few seconds, which makes them very practical.
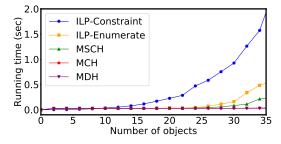

Fig. 10.   Running time of various methods for optimizing FVS.

When it comes to performance (Fig. 11), ILP-based methods have no competition. Interestingly, the simple cycle based method (MSCH) also works quite well and may be useful in place of ILP-based methods for larger problems, given that MSCH runs faster.
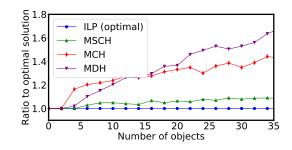

Fig. 11.   Optimality ratio of various methods for optimizing FVS as compared with the optimal ILP-based methods.

The performance is also affected by the average degree for each node, which is directly linked to the complexity of G_{dep}. Fixating on the ILP-Constraint algorithm, experiments with an average degree of 0.5-2.5 are included (2.5 average degree yields rather constrained dependency graphs). As can be observed from Fig. 12, for up to 35 objects, an optimal FVS can be readily computed in a few seconds.
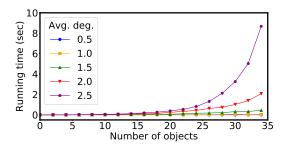

Fig. 12.   The running time of ILP-Constraint under varying G_{dep} average degree. Maximum degree is capped at twice the average degree.

Finally, this section emphasizes an observation regarding the number of optimal FVS sets (Fig. 13). By disabling FVSs that are already obtained in subsequent runs, all FVSs for a given problem can be exhaustively enumerated for varying numbers of objects and average degree of G_{dep}. The number of optimal FVSs turns out to be fairly limited.
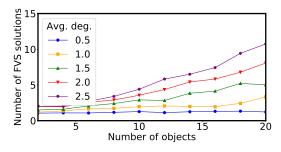

Fig. 13.   The number of optimal FVS solutions in expectation.

C. TORO: Overall Performance

The running time for the entire TOROFVSSINGLE() is provided in Fig. 14. Observe that FVS computation takes almost no time in comparison to the distance minimization step. As expected, higher average degrees in G_{dep} make the computation harder.
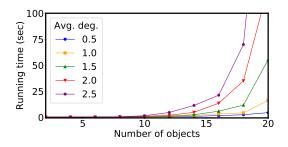
Fig. 14. The total running time for TOROFVSSINGLE().

Running TOROFVSSINGLE() together with FVS enumeration, a global optimal solution is computed for TORO under the assumption that the grasp/release costs dominate. Only solutions with an optimal FVS are considered. The computation time is provided in Fig. 15. The result shows that it gets costly to compute the global optimal solution as the number of objects go beyond 15 for dense setups. It is empirically observed that for the same problem instance and different optimal FVSs, the minimum distance computed by MINDIST() in Alg. 2 has less than 5% variance. This suggests that running TOROFVSSINGLE() just once should yield a solution that is very close to being the global optimum.
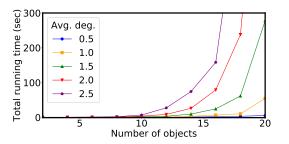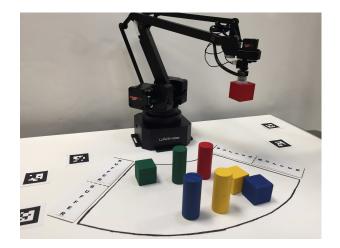

Fig. 15. The running time to produce a global optimal solution for TORO.

VII. PHYSICAL EXPERIMENTS

Fig. 16. A snapshot of the physical system carrying out a solution generated by the algorithms presented in this paper for a tabletop rearrangement scenario.

This section demonstrates an implementation of the algorithms introduced in this paper on a hardware platform

(Fig. 16). The physical experiments were conducted on three different tabletop scenarios. For each scenario, multiple problem instances were generated to compare the efficiency of the solutions produced by the proposed algorithms relative to alternatives, such as random and greedy solutions.

In order to apply object rearrangement algorithms in the physical world, it is first necessary to identify the problem parameters corresponding to the formulation of the TORO problem. Specifically, the algorithms are expecting as input a start and goal arrangement on a tabletop. The goal arrangement is predefined, while the objects are in an initial, arbitrary state. The physical platform first detects the starting arrangement of the objects before executing a solution for rearranging the objects into the desired goal arrangement.

A. Hardware Setup

The experimental setup is comprised of five components:
1. Tabletop The tabletop is a planar surface where the desktop manipulator and objects rest. Clearly defined contours are drawn denoting the projections of the manipulator's reachable area (i.e., workspace), including predefined buffers within this reachable area, as shown in Fig 17.
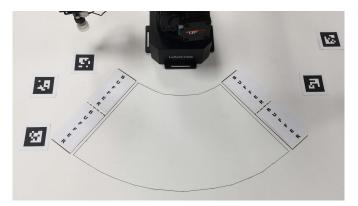

Fig. 17. A tabletop environment where the uArm Swift Pro's workspace is the area between $[45°, 135°]$ at a distance ranging between 140mm and 280mm from the base.

2. Manipulator: The UFACTORY uArm Swift Pro [3] (Fig. 18a) is an inexpensive but versatile desktop manipulator capable of performing repeatable actions with a precision of 0.2mm. The uArm Swift Pro's versatility is largely due to the variety of end-effectors that can be equipped. The suction cup end-effector is utilized to achieve overhand grasps in the forthcoming challenges. Although the uArm Swift Pro is not built for industrial applications, it has enough precision to perform the experimental tasks described in this section.
3. Camera: The Logitech®webcam C920 [4] is a consumer grade webcam capable of Full HD video recording (1080p - 1920×1080 pixels) that is used for object pose detection in the experiments. The camera is mounted above the tabletop, such that it's field-of-view (Fig. 17) captures the entire workspace.

[3]http://www.ufactory.cc/. The authors would like to thank uFactory for supplying the uArm Swift Pro robot that was used in the hardware-based evaluation.

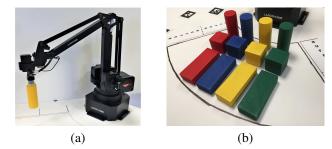[4]https://www.logitech.com/en-us/product/hd-pro-webcam-c920

Fig. 18. (a) The UFACTORY uArm Swift Pro grasping one of the labeled (colored) cylindrical objects. (b) An arrangement of 12 objects of various color and geometry.

The pre-calibration eliminates lens distortion and also renders brighter, saturated images, which makes pose detection easier.

4. Marker Detection "Chilitags" is a cross-platform software library for the detection and identification of two-dimensional fiducial markers [66]. Physical markers placed in the view of the imaging system are used as a point of reference/measure for surrounding objects. In the case of Chilitags, that object is a physical marker added to the environment. As seen in Fig. 17, the experiments employ five tags, each placed at a known pose on the tabletop. This knowledge facilitates the computation of the 2D transformation between the manipulator's frame of reference and the camera's frame of reference.

5. Objects There are several objects that the manipulator interacts with during the experiments (Fig. 18b). These objects are identifiable according to their shape and color

{cube, cylinder, orthotope} × {red, blue, green, yellow}

resulting in twelve uniquely identifiable objects. The center of each object on the tabletop and its orientation define its configuration.

B. Object Pose Detection

The predetermined goal configuration of the objects is defined relative to the manipulator's frame of reference. The initial configuration is unknown and is determined online via the overhead C920 camera. Once the objects are detected, their observed configuration undergoes a transformation to the manipulator's frame of reference.

The pose estimation method appears in Alg. 3. In line 2, an image is taken by the camera. Line 3 utilizes *Gaussian blur* (a.k.a. Gaussian smoothing) to reduce image noise. For each of the predefined colors (i.e., red, blue, yellow, green), the area(s) of the image matching the current color are extracted and further smoothed by *morphological transformations*, including *erosion* and *dilation*. The contours of these areas, which describe the top sides of objects, are then calculated (Line 5). Each contour is examined to determine whether or not it corresponds to one of the objects in the scene (line 7). For each of the contours corresponding to an object in the scene, several operations need to occur to determine pose of the objects. The 2D point component of the pose as it appears in the camera is then determined by computing the center of the contour's minimum enclosing circle (line 9), while the orientation of the object in the camera's frame is extracted via *principle component analysis* over the minimum area rectangle

containing the contour (line 10). Line 11 updates the 2D point component of the pose in the camera's frame to accurately reflect position of the object relative to the manipulator, taking into account the current shape geometry. The 2D perspective transformation between camera frame and robot frame is pre-computed using the marker detection software. The poses of the tags in the robot's frame are fixed, but the pose of the tags in the camera's frame are automatically detected at runtime.

Algorithm 3: OBJECTPOSEESTIMATION

1   $objects \leftarrow \{\}$
2   $img \leftarrow$ CAMERACAPTURE()
3   $img \leftarrow$ GAUSSIANBLUR(img)
4   **for** $color \in \{red, blue, yellow, green\}$ **do**
5     $contours \leftarrow$ FINDCONTOURS($img, color$)
6   **for** $contour \in contours$ **do**
7       $shape \leftarrow$ DETECTSHAPE($contour$)
8   **if** $shape \in \{cube, cylinder, orthotope\}$ **then**
9         $position \leftarrow$ CENTER(MINENCLOSINGCIRCLE($contour$))
10        $orientation \leftarrow$ PCA(MINAREARECT($contour$))
11        $pose \leftarrow$ UPDATE($position, orientation, shape$)
12   **if** INWORKSPACE($pose$) **then**
13          $objects \leftarrow objects \cup \{(shape, color, pose)\}$

14   **return** $objects$
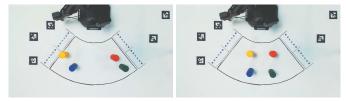

C. Experimental Validation

This section presents three tabletop object rearrangement scenarios that can be performed via overhand pick-and-place actions. For each scenario, specific problem instances have been provided that are solvable. The specific algorithm is determined at run-time, and corresponds to whether there is overlap between the start and goal object configurations. If a subset of the start and goal configurations overlap, the problem may require the use of external buffer(s). The number of extra pick-and-place actions and the corresponding number of buffers necessary to carry out the task, can be determined via the dependency graph.

All of the generated solutions by the proposed methods perform an optimal number of pick-and-place actions. A solution is optimal with respect to the travel distance of the end-effector when the external buffers are not utilized. Problem instances that require the use of an external buffer(s) remain near optimal with respect to the travel distance of the end-effector.

For each problem instance, a feasible solution is also generated by either a random algorithm (for TORO-NO) or a greedy algorithm (for TORO[5]). The execution time for the different solutions are then measured and compared.

Scenario 1: Cylinders without Overlap: This task requires the manipulator arm to transport four uniquely identifiable cylinders from a random start configuration to a fixed

---

[5]The solution produced by the TOROFVSSINGLE algorithm uses the solution returned by the Gurobi ILP solver after 10 sec of compute time. Empirically, any further computation only minimizes the transition time between poses at the expense of increased computation. Note that this does not affect the number of grasps which remain optimal.

(a) Start arrangement   (b) Goal arrangement

Fig. 19. Problem instance of Scenario 1.

Instance	Execution Time (sec)				Difference
	TORONOTSP		Random Solution		
	Raw	Tran	Raw	Tran	
1	65.04	19.81	68.50	23.27	3.46
2	70.44	25.21	75.38	30.15	4.94
3	67.11	21.88	69.85	24.62	2.74
4	69.34	24.11	73.09	27.86	3.75
5	70.67	25.44	73.04	27.81	2.37
6	71.13	25.90	73.37	28.14	2.24
7	73.40	28.17	73.66	28.43	0.26
8	67.95	22.72	67.97	22.74	0.02
9	66.62	21.39	68.21	22.98	1.59
10	66.88	21.65	68.22	22.99	1.34
Average	68.86	23.63	71.13	25.90	2.27

TABLE II
EXPERIMENTAL RESULTS SHOWING A COMPARISON OF THE THE EXECUTION TIME BETWEEN TORONOTSP AND A RANDOM FEASIBLE SOLUTION FOR TEN PROBLEM INSTANCES.

goal configuration. Figures 19a and 19b illustrate one such problem instance where the start and goal configurations do not overlap, indicating that this is a TORO-NO instance. Since TORO-NO does not necessitate the use of any external buffers, the manipulator perform only four pick-and-place operations, corresponding to the number of cylinders in the scene. Appendix C provides the *distance optimal sequence* for pick-and-place operations of this instance.

To illustrate the efficiency of solutions generated by TORONOTSP, 10 different problem instances are generated. They are solved by both TORONOTSP and random grasping sequences. Note that any permutation of objects is a feasible solution. The result is presented in Table II. The first column in this table specifies different problem instances. The *raw* columns measure the total execution time, which contains grasps, releases, and transportation. Since the time for grasps and releases is the same for all the feasible solutions for a TORO-NO instance, the amount of time (45.23 sec) to perform four in-place pick-and-place actions is then deducted from total execution time. These results appear in the *tran* columns. Moreover, the difference between the execution time of the algorithms appear in the *difference* column.

From the empirical data provided in Table II, random solution strategies for this problem setup incur on average a 9.6% increase in transportation time compared to the solution generated by TORONOTSP.

Remark 6. The difference of execution time between a random solution and the optimal solution is generally proportional, but not linearly dependent to the transition cost defined in this paper, which is based on the Euclidean distance between

poses in 2D. This is due to the manipulator model. In practice, the path that the end-effector travels does not necessarily need to be along piece-wise linear shortest paths (straight lines). Additionally, the second order term (acceleration) varies, contributing to a non-static velocity, which is not captured by the tabletop model described herein.
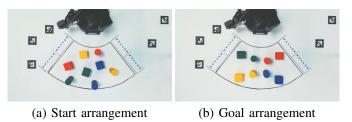

(a) Start arrangement   (b) Goal arrangement

Fig. 20. Problem instance of Scenario 2.

Scenario 2: Cylinders and Cubes: In this scenario, the arm is tasked with rearranging eight objects (four cylinders and four cubes) that are initially scattered throughout the workspace, while the desired goal configuration is predetermined. Figures 20a and 20b show one such instance. Due to overlap between the start and goal configurations, this is a TORO instance and thus uses the TOROFVSSINGLE algorithm, making use of the external buffers available to the manipulator. In the solution of TOROFVSSINGLE on this particular instance, the manipulator uses one of the available buffer locations to perform the rearrangement. The movement of an object to an external buffer results in a total of nine pick-and-place actions.

TOROFVSSINGLE is compared to a greedy method, which solves the problems sequentially by first removing the dependencies for one object and then it moves it to its goal. As shown in Table III, the greedy algorithm returns 1 extra grasps and takes 24.45 secs of additional execution time, compared to TOROFVSSINGLE.
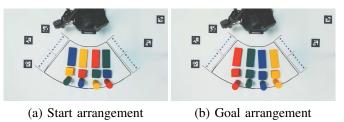

(a) Start arrangement   (b) Goal arrangement

Fig. 21. Problem instance for Scenario 3 containing twelve objects.

Scenario 3: Cylinders, Cubes, Orthotopes: This scenario involves rearranging twelve objects (four of each type of cylinders, cubes and orthotopes) within the manipulator's workspace. Objects of identical geometry are aligned in front of the manipulator, ordered by increasing height (i.e., orthotopes, cubes, cylinders). Thus, start and goal configurations differ by permutations of color amongst objects of the same shape. The instance shown in Figures 21a and 21b utilizes three of the available buffer locations as it performs sixteen pick-and-place actions necessary to solve the task.

As the number of objects increases, the difference between the solution quality of TOROFVSSINGLE and the greedy algorithm becomes larger. The solution of greedy algorithm has

Scenario	Execution Time (sec)		Num. of Actions	
	TOROFVSSINGLE	Greedy Alg.	TOROFVSSINGLE	Greedy Alg.
2	165.57	190.02	9	10
3	299.95	405.16	16	20

TABLE III
EXPERIMENTAL RESULTS SHOWING A COMPARISON OF THE THE EXECUTION TIME BETWEEN TOROFVSSINGLE AND A GREEDY SOLUTION FOR TWO SCENARIOS.

4 extra grasps and 105.21 secs more execution time compared to the sub-optimal solution generated by TOROFVSSINGLE.

VIII. CONCLUSION

This paper studies the combinatorial structure inherent in tabletop object rearrangement problems. For TORO-NO and TORO-UNO, it is shown that Euclidean-TSP can be reduced to them, establishing their NP-hardness. More importantly, TORO-NO and TORO-UNO can be reduced to TSP with little overhead, thus establishing that they have similar computational complexity and lead to an efficient solution scheme. Similarly, an equivalence was established between dependence breaking of TORO and FVS, which is APX-hard. The equivalence enables subsequent ILP-based methods for effectively and optimally solving TORO instances containing tens of objects with overlapping starts and goals.

The methods and algorithms in this paper serve as an initial foundation for solving complex rearrangement tasks on tabletops. Many interesting problems remain open in this area; two are highlighted here. The current paper assumes the availability of *external* buffers, which are separated from the workspace occupied by the objects, demanding additional movement from the end-effector. In practice, it can be beneficial to dynamically locate buffers that are close by, which may be tackled through effective sampling methods. Furthermore, the scenarios addressed only static settings whereas many industrial settings require solving a more dynamics problem in which the objects to be rearranged do not remain still with respect to the robot base.

APPENDIX

Proof of Theorem IV.2: Again, reduce from Euclidean-TSP. The same TSP instance from the proof of Theorem IV.1 is used. The conversion to TORO-NO and the process to obtain a TORO-UNO instance are also similar, with the exception being that edges $s_i g_i$ are not required to be used in a solution; this makes the labeled case become unlabeled.

The argument is that the cost-optimal solution of the TORO-UNO instance also yields an optimal solution to the original Euclidean-TSP tour. This is accomplished by showing that an optimal solution to the TORO-NO instance has essentially the same cost as the TORO-UNO instance. To see that this is the case, assume that an optimal solution (tour) path to the reduced TORO-UNO problem is given. Let the path have a total length (cost) of $D_{opt}^{\text{TORO-UNO}}$. Let $s_i g_i$ be the first such edge that is not in the TORO-UNO solution. Because the path is a tour, following s_i along the path will eventually reach g_i. The resulting path will have the form $s_i v_1 \ldots v_2 g_i v_3$, i.e., the black path in Fig. 22.
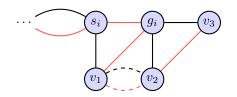

Fig. 22. Augmenting a path in an TORO-UNO solution.

Upon the observation of such a partial solution, proceed to make the augmentation and replace the path with the new one (red path in Fig. 22). Because $s_i g_i \ll 1/(4n)$, the potential increase in path length is bounded by (note that $v_2 v_3$ is shorter than the additive length of $v_2 g_i$ and $g_i v_3$)

$$\|s_i g_i\|_2 + \|g_i v_1\|_2 - \|s_i v_1\|_2 \leq 2\varepsilon \ll 1/(2n).$$

After at most n such augmentations, an optimal TORO-UNO solution is converted to an TORO-NO solution. The TORO-NO solution has a cost increase of at most $n * 1/(2n) = 1/2$. The TORO-NO solution can then be converted to a solution of the Euclidean-TSP problem, which will not increase the cost. Thus, a TORO-UNO solution can be converted to a corresponding Euclidean-TSP solution with a cost addition of less than $1/2$. Let the Euclidean-TSP solution obtained in this manner have a total cost of D', then

$$D' < D_{opt}^{\text{TORO-UNO}} + \frac{1}{2}. \tag{4}$$

Now again let the optimal Euclidean-TSP solution have a cost of D_{opt}. The solution can be converted to an TORO-NO solution with a total cost of less than $D_{opt} + 1/4$. The TORO-NO solution is also a solution to the TORO-UNO problem. That is, for this new TORO-UNO solution, the cost is

$$D^{\text{TORO-UNO}} < D_{opt} + \frac{1}{4}. \tag{5}$$

Now, if $D' > D_{opt}$, then $D' \geq D_{opt} + 1$. Putting this together with (4) and (5),

$$D^{\text{TORO-UNO}} < D_{opt} + \frac{1}{4} \leq D' - \frac{3}{4} \leq D_{opt}^{\text{TORO-UNO}} - \frac{1}{4},$$

which is a contradiction. Therefore, $D' > D_{opt}$ cannot be true. Therefore, a cost-optimal TORO-UNO solution yields an optimal solution to the original Euclidean-TSP problem. This shows that TORO-UNO is at least as hard as Euclidean-TSP. ∎

To compute the exact solution, the problem is modeled as an ILP problem, and then solved using LP solvers, e.g., Gurobi TSP Solver [65]. In this paper, two different ILP models are

used, which are similar to the models introduced in sections 3.1 and 3.2 of [64]:

1) **ILP-Constraint.** By splitting all vertices $o_i \in G_{dep}$ to o_i^{in} and o_i^{out}, a new graph $G_{arc}(V_{arc}, E_{arc})$ is constructed, where $V_{arc} = \{o_1^{in}, o_1^{out}, \ldots, o_n^{in}, o_n^{out}\}$, and $(o_i^{out}, o_j^{in}) \in E_{arc}$ iff $(o_i, o_j) \in A_{dep}$. By adding extra edges (o_i^{in}, o_i^{out}) for all $1 \le i \le n$ to E_{arc}, problem is transformed to a *minimum feedback arc set* problem, where the objective is to find a minimum set of arcs to make G_{arc} acyclic. Moreover, every edge in this set ends at o_i^{in} or starts from o_i^{out} can be replaced by (o_i^{in}, o_i^{out}), which stands for a vertex o_i in G_{dep}, without changing the feasibility of the solution.

The next step is to find a minimum cost ordering π^* of the nodes in G_{arc}. Let $c_{i,j} = 1$ if edge $(i, j) \in E_{arc}$, while $c_{i,j} = 0$ if edge $(i, j) \notin E_{arc}$. Furthermore, let binary variables $y_{i,j}$ associate the ordering of $i, j \in \pi$, where $y_{i,j} = 0$ if i precedes j, or 1 if j precedes i. Suppose $|V_{arc}| = m$, the LP formulation is expressed as:

$$\min_y \quad \sum_{j=1}^{m}\left(\sum_{k=1}^{j-1} c_{k,j} y_{k,j} + \sum_{l=j+1}^{n} c_{l,j}(1 - y_{j,l})\right)$$

$$\text{s.t.} \quad y_{i,j} + y_{j,k} - y_{i,k} \le 1, \quad 1 \le i < j < k \le m$$
$$-y_{i,j} - y_{j,k} + y_{i,k} \le 0, \quad 1 \le i < j < k \le m$$

The solution arc set contains all the backward edges in π^*.

2) **ILP-Enumerate.** First find the set C of all the simple cycles in G_{dep}. A set of binary variables $V = \{v_1, \ldots, v_n\}$ is defined, each assigned to an object $o_i \in O$, the LP formulation is expressed as::

$$\max_v \quad \sum_{v_i \in V} v_i$$
$$\text{s.t.} \quad \sum_{o_i \in C_j} v_i < |C_j|, \quad \forall C_j \in C.$$

Then the vertices in the minimum FVS is the objects whose corresponding variable v_i is 0 in the solution of this LP model.

Given a TORO instance with n objects $\mathcal{O} = \{o_1, \ldots, o_n\}$, without loss of generality, $B = \{o_1, \ldots, o_p\} \subset \mathcal{O}$ denotes the set of objects to be moved to buffers, which is calculated by the methods introduced in Section V-B and Appendix A. The maximum number of buffers to be used is denoted as $p = |B|$. The ILP model introduced in this section finds the distance-optimal solution amongst all candidates that moves objects in B to intermediate locations before moving them to goal configurations while employing the minimum number of grasps (i.e. $n + p$).

All variables in this ILP model are boolean variables, and have two components: *nodes* and *edges*, where a node denotes the occupancy of a position on the tabletop at a specific time step, and an edge represents a movement of the manipulator between two positions. The variables appear as a repeated graph pattern in a discrete time domain $t \in \{0, \ldots, n + p\}$,

where time step t correlates to the states of the system after the tth pick-and-place action.

Assume the following:

$$\begin{aligned} 1 &\le i &\le n, \\ 1 &\le j &\le p, \\ 1 &\le k &\le p, \\ 1 &\le \ell &\le n, \\ p &< m &\le n. \end{aligned}$$

A. Variables: Nodes

There are three kinds of nodes:

- $\{s_1^t, \ldots, s_n^t\}$, occupancy of start configurations. $s_i^t = 1$ indicates o_i is at its start configuration at time step t.
- $\{g_1^t, \ldots, g_n^t\}$, occupancy of goal configurations. $g_i^t = 1$ indicates o_i is at its goal configuration at time step t.
- $\{b_{11}^t, b_{12}^t, \ldots, b_{pp}^t\}$, occupancy of buffers. $b_{jk}^t = 1$ indicates o_j is in buffer b_k at time step t.
- s_M, g_M, indicate the occupancy of the manipulator's rest positions.

The value of the nodes when $t = 0$ and $t = n + p$ indicate the start and goal arrangement, respectively. Specifically,

$$\begin{aligned} s_i^0 &= 1, & g_i^0 &= 0, & b_{jk}^0 &= 0, \\ s_i^{n+p} &= 0, & g_i^{n+p} &= 1, & b_{jk}^{n+p} &= 0. \end{aligned}$$

B. Variables: Edges

Edges model the movement of the manipulator and are included in the cost function. An edge connects two nodes, e.g. node 1 and 2, and is denoted as $e(12)$. Edges in the ILP model are listed as follows.

- $e(s_m^t g_m^t)$, for $1 \le t \le n + p$. A positive value indicates a pick-and-place action that brings o_m from its start configuration to its goal configuration at time step t.
- $e(s_j^t b_{jk}^t)$, $e(b_{jk}^t g_j^t)$, for $1 \le t \le n + p$. A positive value indicates a pick-and-place action that brings o_j from its start configuration to buffer k, and from buffer k to its goal configuration.
- $e(g_i^t s_\ell^{t+1})$, $e(b_{jk}^t s_i^{t+1})$, $e(g_i^t b_{jk}^{t+1})$, for $1 \le t < n + p$, indicates a movement of the manipulator without an object being grasped.
- $e(s_M s_i^1)$, $e(g_i^{n+p} g_M)$, denote the target objects of the first and the last pick-and-place actions.

Note that because each edge is associated with a movement of the manipulator, the total travel distance of the end-effector can be modeled as the summation of the value (i.e. 0 or 1) of all edges multiplied with the cost associated with the edge. The objective of this ILP model is

$$\min \sum_e \text{cost}(e),$$

where $\text{cost}(e)$ denotes the distance between positions associated with nodes connected by edge e.

An illustration of the ILP model is provided in Fig. 23.

C. Constraints

This section addresses the constraints that appear in the ILP model. These constraints update the value of variables, which ensures that the solution returned by the ILP model is able to be reduced to a feasible solution for the original TORO.
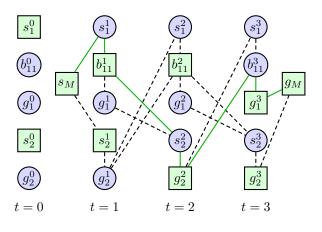

Fig. 23. An example of ILP model when $n = 2, p = 1$ as well as value of variables after solving this model. The green square nodes and green solid edges indicate the value of variables is 1. The solution is interpreted as (i) bring o_1 to a buffer, (ii) bring o_2 to its goal, (iii) bring o_1 to its goal.

Begin by considering the constraints of the first pick-and-place action. To update the occupancy of start configurations:

$$\sum_{i=1}^{n} e(s_M s_i^1) = s_M = 1, \quad s_i^1 = s_i^0 - e(s_M s_i^1).$$

To update the occupancy of buffers and goal configurations:

$$\sum_{k=1}^{p} e(s_j^1 b_{jk}^1) = e(s_M s_j^1), b_{jk}^1 = b_{jk}^0 + e(s_j^1 b_{jk}^1),$$
$$e(s_m^1 g_m^1) = e(s_M s_m^1), g_m^1 = g_m^0 + e(s_m^1 g_m^1).$$

After this step, the constraints for all other time steps can be modeled. Assume the following: $1 \le t \le n + p - 1$.

The movement of the manipulator between time step t and $t + 1$ correspond to:

$$e(s_j^t b_{jk}^t) = \sum_{i=1}^{n} e(b_{jk}^t s_i^{t+1}) + \sum_{a=1}^{p}\sum_{b=1}^{p} e(b_{jk}^t b_{ab}^{t+1}),$$
$$\sum_{j=1}^{p} e(b_{jk}^t g_j^t) = \sum_{i=1}^{n} e(g_j^t s_i^{t+1}) + \sum_{k=1}^{p}\sum_{l=1}^{p} e(g_j^t b_{kl}^{t+1}),$$
$$e(s_m^t g_m^t) = \sum_{i=1}^{n} e(g_m^t s_i^{t+1}) + \sum_{k=1}^{p}\sum_{l=1}^{p} e(g_j^t b_{kl}^{t+1}).$$

For time step $t+1$, constraints are imposed on the incoming edges from time step t, in order to avoid the scenario where the manipulator travels to a vacant location:

$$\sum_{i=1}^{n} e(g_i^t s_\ell^{t+1}) + \sum_{j=1}^{p}\sum_{k=1}^{p} e(b_{jk}^t s_\ell^{t+1}) \le s_\ell^t,$$
$$\sum_{i=1}^{n} e(g_i^t b_{jk}^{t+1}) + \sum_{a=1}^{p}\sum_{b=1}^{p} e(b_{ab}^t b_{jk}^{t+1}) \le b_{jk}^t.$$

Update the edges to simulate a pick-and-place action in time step $t + 1$:

$$\sum_{k=1}^{p} e(s_j^{t+1} b_{jk}^{t+1}) = \sum_{i=1}^{n} e(g_i^t s_j^{t+1}) + \sum_{a=1}^{p}\sum_{b=1}^{p} e(b_{ab}^t s_j^{t+1}),$$
$$e(b_{jk}^{t+1} g_j^{t+1}) = \sum_{i=1}^{n} e(g_i^t b_{jk}^{t+1}) + \sum_{a=1}^{p}\sum_{b=1}^{p} e(b_{ab}^t b_{jk}^{t+1}),$$
$$e(s_m^{t+1} g_m^{t+1}) = \sum_{i=1}^{n} e(g_i^t s_m^{t+1}) + \sum_{j=1}^{p}\sum_{k=1}^{p} e(b_{jk}^t s_m^{t+1}).$$

Update nodes in time step $t + 1$:

$$s_i^{t+1} = s_i^t - \sum_{\ell=1}^{n} e(g_\ell^t s_i^{t+1}) - \sum_{j=1}^{p}\sum_{k=1}^{p} e(b_{jk}^t s_i^{t+1}),$$
$$b_{jk}^{t+1} = b_{jk}^t + e(s_j^{t+1} b_{jk}^{t+1})$$
$$- \sum_{i=1}^{n} e(g_i^t b_{jk}^{t+1}) - \sum_{a=1}^{p}\sum_{b=1}^{p} e(b_{ab}^t b_{jk}^{t+1}),$$

$$g_j^{t+1} = g_j^t + \sum_{k=1}^{p} e(b_{jk}^{t+1} g_j^{t+1}),$$
$$g_m^{t+1} = g_m^t + e(s_m^{t+1} g_m^{t+1}).$$

Since each buffer is presented as multiple copies in each time step, one must make sure it is occupied by at most one object:

$$\sum_{j=1}^{p} b_{jk}^t \le 1.$$

Update the dependencies in the dependency graph. Suppose s_i is in collision with g_ℓ then

$$s_i^t + g_\ell^t \le 1.$$

After employed all $n + p$ pick-and-place actions, the manipulator goes to the rest position g_M:

$$e(g_j^{n+p} g_M) = \sum_{k=1}^{p} e(b_{jk}^{n+p} g_j^{n+p}),$$
$$e(g_m^{n+p} g_M) = e(s_m^{n+p} g_m^{n+p}),$$
$$g_M = \sum_{j=1}^{p} e(g_j^{n+p} g_M) + \sum_{m=p+1}^{n} e(g_m^{n+p} g_M) = 1.$$

Fig. 24 demonstrates the optimal solution for the problem instance shown in Fig. 19. The sequence of pick-and-place actions over the colored cylinders are yellow, red, green, blue.

Fig. 24.   Step by step solution for the `TORO-NO` instance in Fig. 19.

REFERENCES

[1] C. H. Papadimitriou, "The Euclidean travelling salesman problem is NP-complete," *Theoretical Computer Science*, vol. 4, no. 3, pp. 237–244, 1977.

[2] J. van den Berg, J. Snoeyink, M. Lin, and D. Manocha, "Centralized path planning for multiple robots: Optimal decoupling into sequential plans," in *Proc. Robotics: Science and Systems*, 2009.

[3] R. M. Karp, "Reducibility among combinatorial problems," in *Complexity of computer computations*. Springer, 1972, pp. 85–103.

[4] M. F. E. Rohmer, S. P. N. Singh, "V-REP: a Versatile and Scalable Robot Simulation Framework," in *Proc. IEEE/RSJ International Conference on Intelligent Robots and Systems*, 2013.

[5] I. Dinur and S. Safra, "On the hardness of approximating minimum vertex cover," *Annals of Mathematics*, pp. 439–485, 2005.

[6] K. Treleaven, M. Pavone, and E. Frazzoli, "Asymptotically optimal algorithms for one-to-one pickup and delivery problems with applications to transportation systems," *IEEE Transactions on Automatic Control*, vol. 58, no. 9, pp. 2261–2276, 2013.

[7] S. D. Han, N. M. Stiffler, A. Krontiris, K. E. Bekris, and J. Yu, "High-Quality Tabletop Rearrangement with Overhand Grasps: Hardness Results and Fast Methods," in *Proc. Robotics: Science and Systems*, Boston, Massachusetts, U.S.A., Jul. 2017.

[8] B. Aronov, M. de Berg, A. F. van den Stappen, P. Švestka, and J. Vleugels, "Motion Planning for Multiple Robots," *Discrete and Computational Geometry*, vol. 22, no. 4, pp. 505–525, 1999.

[9] K. Solovey, J. Yu, O. Zamir, and D. Halperin, "Motion Planning for Unlabeled Discs with Optimality Guarantees," in *Proc. Robotics: Science and Systems*, 2015.

[10] K. Solovey and D. Halperin, "On the hardness of unlabeled multi-robot motion planning," in *Proc. Robotics: Science and Systems*, 2015.

[11] J. van den Berg and M. Overmars, "Prioritized Motion Planning for Multiple Robots," in *Proc. IEEE/RSJ International Conference on Intelligent Robots and Systems*, 2005, pp. 2217–2222.

[12] S. Leroy, J.-P. Laumond, and T. Siméon, "Multiple Path Coordination for Mobile Robots: A Geometric Algorithm," in *Proc. International Joint Conferences on Artificial Intelligence*, 1999, pp. 1118–1123.

[13] R. H. Wilson and J.-C. Latombe, "Geometric Reasoning about Mechanical Assembly," *Artificial Intelligence*, vol. 71, no. 2, pp. 371–396, 1994.

[14] D. Halperin, J.-C. Latombe, and R. H. Wilson, "A General Framework for Assembly Planning: the Motion Space Approach," *Algorthmica*, vol. 26, no. 3-4, pp. 577–601, 2000.

[15] S. Sundaram, I. Remmler, and N. M. Amato, "Disassembly Sequencing Using a Motion Planning Approach," in *Proc. IEEE International Conference on Robotics and Automation*, Washington, D.C., May 2001, pp. 1475–1480.

[16] D. Kornhauser, G. Miller, and P. Spirakis, "Coordinating Pebble Motion on Graphs, the Diameter of Permutation Groups, and Applications," in *Proc. IEEE Symposium on Foundations of Computer Science*, 1984, pp. 241–250.

[17] G. Calinescu, A. Dumitrescu, and J. Pach, "Reconfigurations in Graphs and Grids," *SIAM Journal on Discrete Mathematics*, vol. 22, no. 1, pp. 124–138, 2008.

[18] V. Auletta, A. Monti, D. Parente, and G. Persiano, "A Linear Time Algorithm for the Feasibility of Pebble Motion on Trees," *Algorthmica*, vol. 23, pp. 223–245, 1999.

[19] G. Goraly and R. Hassin, "Multi-Color Pebble Motion on Graphs," *Algorthmica*, vol. 58, no. 3, pp. 610–636, 2010.

[20] G. Wagner, M. Kang, and H. Choset, "Probabilistic Path Planning for Multiple Robots with Subdimensional Expansion," in *Proc. IEEE International Conference on Robotics and Automation*, 2012.

[21] G. Sharon, R. Stern, A. Felner, and N. R. Sturtevant, "Conflict-based Search for Optimal Multi-agent Pathfinding," in *Artificial Intelligence*, no. 219, 2015, pp. 40–66.

[22] J. Yu and S. M. LaValle, "Multi-agent Path Planning and Network Flow," in *Proc. Workshop on the Algorithmic Foundations of Robotics*, 2012.

[23] ——, "Optimal Multi-Robot Path Planning on Graphs: Complete Algorithms and Effective Heuristics," *IEEE Transactions on Robotics*, vol. 32, no. 5, pp. 1163–1177, 2016.

[24] G. Wilfong, "Motion Planning in the Presence of Movable Obstacles," in *Annals of Mathematics and Artificial Intelligence*, 1991, pp. 131–150.

[25] P. C. Chen and Y. K. Hwang, "Practical Path Planning Among Movable Obstacles," in *Proc. IEEE International Conference on Robotics and Automation*, May 1991, pp. 444–449.

[26] E. Demaine, J. O'Rourke, and M. L. Demaine, "Pushpush and push-1 are NP-hard in 2D," in *Proc. Candadian Conference on Computational Geometry*, 2000, pp. 211–219.

[27] D. Nieuwenhuisen, A. F. van der Stappen, and M. H. Overmars, "An Effective Framework for Path Planning amidst Movable Obstacles," in *Proc. Workshop on the Algorithmic Foundations of Robotics*, 2006.

[28] J. van den Berg, M. Stilman, J. J. Kuffner, M. Lin, and D. Manocha, "Path Planning Among Movable Obstacles: A Probabilistically Complete Approach," in *Proc. Workshop on the Algorithmic Foundations of Robotics*, 2008.

[29] M. Stilman, J. Schamburek, J. J. Kuffner, and T. Asfour, "Manipulation Planning Among Movable Obstacles," in *Proc. IEEE International Conference on Robotics and Automation*, 2007.

[30] O. Ben-Shahar and E. Rivlin, "Practical Pushing Planning for Rearrangement Tasks," *IEEE Transactions on Robotics and Automation*, vol. 14, no. 4, Aug. 1998.

[31] J. Ota, "Rearrangement Planning of Multiple Movable Objects," in *Proc. IEEE International Conference on Robotics and Automation*, 2004.

[32] G. Havur, G. Ozbilgin, E. Erdem, and V. Patoglu, "Geometric Rearrangement of Multiple Moveable Objects on Cluttered Surfaces: A Hybrid Reasoning Approach," in *Proc. IEEE International Conference on Robotics and Automation*, 2014.

[33] S. Srivastava, E. Fang, L. Riano, R. Chitnis, S. Russell, and P. Abbeel, "Combined Task and Motion Planning through an Extensible Planner-Independent Interface Layer," in *Proc. IEEE International Conference on Robotics and Automation*, 2014.

[34] C. R. Garrett, T. Lozano-Pérez, and L. P. Kaelbling, "FFRob: An efficient heuristic for task and motion planning," in *Proc. Workshop on the Algorithmic Foundations of Robotics*, 2014.

[35] A. Krontiris, R. Shome, A. Dobson, A. Kimmel, and K. E. Bekris, "Rearranging Similar Objects with a Manipulator using Pebble Graphs," in *Proc. IEEE International Conference on Humanoid Robotics*, Madrid, Spain, 2014.

[36] A. Krontiris and K. E. Bekris, "Dealing with Difficult Instances of Object Rearrangement," in *Proc. Robotics: Science and Systems*, Rome, Italy, Jul. 2015.

[37] ——, "Efficiently Solving General Rearrangement Tasks: A Fast Extension Primitive for an Incremental Sampling-based Planner," in *Proc. IEEE International Conference on Robotics and Automation*, Sweden, 2016.

[38] K. Hauser, "The Minimum Constraint Removal Problem with Three Robotics Applications," *International Journal of Robotics Research*, vol. 33, no. 1, pp. 5–17, 2014.

[39] G. Berbeglia, J.-F. Cordeau, I. Gribkovskaia, and G. Laporte, "Static pickup and delivery problems: a classification scheme and survey," *Top*, vol. 15, no. 1, pp. 1–31, 2007.

[40] G. Berbeglia, J.-F. Cordeau, and G. Laporte, "Dynamic pickup and delivery problems," *European Jornal of Operational Research*, vol. 202, no. 1, pp. 8–15, 2010.

[41] G. Laporte, "The vehicle routing problem: An overview of exact and approximate algorithms," *European Jornal of Operational Research*, vol. 59, no. 3, pp. 345–358, 1992.

[42] N. Christofides and S. Eilon, "An algorithm for the vehicle-dispatching problem," *Journal of the Operational Research Society*, vol. 20, no. 3, pp. 309–318, 1969.

[43] M. R. Garey and D. S. Johnson, *Computers and Intractability: A Guide to the Theory of NP-Completeness*. W. H. Freeman, 1979.

[44] S. Anily and R. Hassin, "The swapping problem," *Networks*, vol. 22, no. 4, pp. 419–433, 1992.

[45] P. Beullens, D. van Oudheusden, and L. N. van Wassenhove, "Collection and vehicle routing issues in reverse logistics," in *Reverse Logistics*. Springer, 2004, pp. 95–134.

[46] A. Hoff and A. Løkketangen, "Creating lasso-solutions for the traveling salesman problem with pickup and delivery by tabu search," *Central European Journal of Operations Research*, vol. 14, no. 2, pp. 125–140, 2006.

[47] I. Gribkovskaia, Ø. Halskau, G. Laporte, and M. Vlček, "General solutions to the single vehicle routing problem with pickups and deliveries," *European Journal of Operational Research*, vol. 180, no. 2, pp. 568–584, 2007.

[48] G. N. Frederickson, M. S. Hecht, and C. E. Kim, "Approximation algorithms for some routing problems," in *17th Annual Symposium on Foundations of Computer Science (sfcs 1976)*. IEEE, 1976, pp. 216–227.

[49] T. Siméon, J.-P. Laumond, J. Cortés, and A. Sahbani, "Manipulation Planning with Probabilistic Roadmaps," *International Journal of Robotics Research*, no. 23, 2004.

[50] D. Berenson, S. S. Srinivasa, and J. J. Kuffner, "Task Space Regions: A Framework for Pose-Constrained Manipulation Planning," *International Journal of Robotics Research*, vol. 30, no. 12, pp. 1435–1460, 2012.

[51] J. B. Cohen, S. Chitta, and M. Likhachev, "Single- and Dual-arm Motion Planning with Heuristic Search," in *International Journal of Robotics Research*, 2013.

[52] M. Zucker, N. Ratliff, A. Dragan, M. Pivtoraiko, M. Klingensmith, C. Dellin, J. A. Bagnell, and S. S. Srinivasa, "CHOMP: Covariant Hamiltonian Optimization for Motion Planning," *International Journal of Robotics Research*, 2013.

[53] M. Ciocarlie and P. Allen, "Hand Posture Subspaces for Dexterous Robotic Grasping," in *International Journal of Robotics Research*, vol. 28, no. 7, 2009.

[54] J. Bohg, A. Morales, T. Asfour, and D. Kragic, "Data-driven Grasp Synthesis - A Survey," in *IEEE Transactions on Robotics*, vol. 30, no. 2, Apr. 2014.

[55] A. Cosgun, T. Hermans, V. Emeli, and M. Stilman, "Push Planning for Object Placement on Cluttered Table Surfaces," in *Proc. IEEE/RSJ International Conference on Intelligent Robots and Systems*, 2011.

[56] M. R. Dogar and S. S. Srinivasa, "A Framework for Push-Grasping in Clutter," in *Proc. Robotics: Science and Systems*, 2011.

[57] S. Cambon, R. Alami, and F. Gravot, "A Hybrid Approach to Intricate Motion, Manipulation, and Task Planning," *International Journal of Robotics Research*, no. 28, 2009.

[58] E. Plaku and G. Hager, "Sampling-based motion and symbolic action planning with geometric and differential constraints," in *Proc. IEEE International Conference on Robotics and Automation*, 2010.

[59] M. Gharbi, R. Lallement, and R. Alami, "Combining symbolic and geometric planning to synthesize human-aware plans: toward more efficient combined search," in *Proc. IEEE/RSJ International Conference on Intelligent Robots and Systems*, 2015, pp. 6360–6365.

[60] N. T. Dantam, Z. K. Kingston, S. Chaudhuri, and L. E. Kavraki, "Incremental Task and Motion Planning: A Constraint-Based Approach," in *Proc. Robotics: Science and Systems*, 2016.

[61] W. Vega-Brown and N. Roy, "Asymptotically optimal planning under piecewise-analytic constraints," in *Proc. Workshop on the Algorithmic Foundations of Robotics*, 2016.

[62] G. N. Frederickson and D. J. Guan, "Nonpreemptive ensemble motion planning on a tree," *Journal of Algorithms*, vol. 15, no. 1, pp. 29–60, 1993.

[63] D. L. Applegate, R. E. Bixby, V. Chvatal, and W. J. Cook, *The Traveling Salesman Problem: A Computational Study*. Princeton, NJ, USA: Princeton University Press, 2007.

[64] A. Baharev, H. Schichl, and A. Neumaier, "an exact method for the minimum feedback arc set problem," *University of Vienna*, vol. 10, pp. 35–60, 2015.

[65] I. Gurobi Optimization, "Gurobi Optimizer Reference Manual," 2016. [Online]. Available: http://www.gurobi.com

[66] Q. Bonnard, S. Lemaignan, G. Zufferey, A. Mazzei, S. Cuendet, N. Li, A. Özgür, and P. Dillenbourg, "Chilitags 2: Robust Fiducial Markers for Augmented Reality and Robotics," 2013. [Online]. Available: http://chili.epfl.ch/software